

## Direct photon production at the $\psi$

D. L. Scharre, M. S. Alam,\* A. M. Boyarski, M. Breidenbach, D. L. Burke, J. Dorenbosch, J. M. Dorfan, G. J. Feldman, M. E. B. Franklin, G. Hanson, K. G. Hayes, T. Himel,<sup>†</sup> D. G. Hitlin,<sup>†</sup> R. J. Hollebeek, W. R. Innes, J. A. Jaros, P. Jenni,<sup>†</sup> V. Lüth, M. L. Perl, B. Richter, A. Roussarie, R. H. Schindler,<sup>†</sup> R. F. Schwitters,<sup>§</sup> J. L. Siegrist, H. Taureg,<sup>†</sup> M. Tonutti,<sup>||</sup> R. A. Vidal, J. M. Weiss, and H. Zaccone<sup>¶</sup>  
*Stanford Linear Accelerator Center, Stanford University, Stanford, California 94305*

G. S. Abrams, C. A. Blocker, W. C. Carithers, M. W. Coles, S. Cooper, W. E. Dieterle, J. B. Dillon, M. W. Eaton, G. Gidal, G. Goldhaber, A. D. Johnson, J. A. Kadyk, A. J. Lankford, R. E. Millikan, M. E. Nelson, C. Y. Pang, J. F. Patrick, J. Strait, G. H. Trilling, E. N. Vella, and I. Videau

*Lawrence Berkeley Laboratory and Department of Physics, University of California, Berkeley, California 94720*

(Received 15 July 1980)

We present results of a detailed analysis of inclusive direct photon production at the  $\psi(3095)$ . The direct-photon momentum distribution for  $x > 0.4$  is presented and compared with the leading-order quantum-chromodynamic prediction. The total production rate is found to be consistent with theoretical expectations, but the observed momentum distribution is considerably softer. Results of an analysis of some inclusive properties of the hadronic system recoiling against the direct photon are presented. The mean charged-particle and  $K_S$  multiplicities are presented as functions of the invariant mass of the hadronic system. These data agree well with the corresponding mean multiplicities measured in  $e^+e^-$  annihilations at center-of-mass energies comparable to the invariant mass of the hadronic system.

### I. INTRODUCTION

In a previous Letter<sup>1</sup> we reported on a measurement of direct photon production at the  $\psi(3095)$ .<sup>2</sup> In this article, we present a detailed discussion of the analysis and the results. Results of two alternate, independent methods of analysis are presented which are consistent with the previously presented results. In addition, we present an analysis of some inclusive properties of the hadronic system recoiling against the direct photon. In particular, we have measured the mean charged-particle and  $K_S$  multiplicities as functions of the invariant mass of the hadronic system. A comparison is made between these data and the corresponding mean multiplicities measured in  $e^+e^-$  annihilations at center-of-mass energies comparable to the invariant mass of the hadronic system.

Leading-order quantum-chromodynamics (QCD) calculations predict that a significant fraction of the hadronic decays of heavy-quark-antiquark  $^3S_1$  resonances (such as the  $\psi$ ) result in the production of direct photons (i.e., photons not coming from secondary decays of  $\pi^0$ 's or  $\eta$ 's).<sup>3</sup> The hadronic decays of the  $\psi$  are assumed to proceed via an intermediate state consisting of at least three color-octet gluons. The lowest-order QCD diagram corresponds to the three-gluon decay shown in Fig. 1(a). By replacing one of the outgoing gluon lines with a photon, as in Fig. 1(b), one obtains a diagram which results in the production of direct photons. This diagram is expected to provide the dominant contribution to

direct photon production. A calculation of the ratio of the partial widths to these two final states gives

$$B_\gamma = \frac{\Gamma(\psi \rightarrow \gamma gg)}{\Gamma(\psi \rightarrow ggg)} = \frac{36}{5} \left( \frac{\alpha}{\alpha_s} \right) (e_Q)^2,$$

where  $\frac{36}{5}$  is a color-SU(3) factor,  $e_Q$  is the charge of the charmed quark, and  $\alpha_s$  is the color fine-structure constant. For  $\alpha_s = 0.18$ ,<sup>4</sup> one calculates  $B_\gamma = 0.13$ . Equating the direct decay of the  $\psi$  into hadrons with the three-gluon decay, and correcting for second-order electromagnetic decays, the lowest-order QCD prediction for the branching ratio into final states with a direct photon is  $B(\psi \rightarrow \gamma + X) = 0.08$ .

The momentum spectrum for  $\gamma$ 's produced in such decays is calculated to be roughly proportional to  $x$ , where  $x$  is the fraction of the beam energy taken by the  $\gamma$ , and peaks near  $x=1$  (see Fig. 2). The dashed curve shows the expected modification of the spectrum in the event of resonance production (either gluon bound states or normal  $q\bar{q}$  states which couple to the two-gluon system) in the final state. However, it must be remembered that this calculation includes only

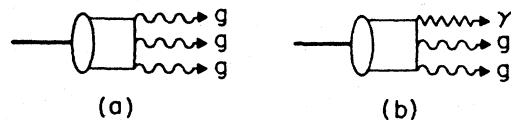


FIG. 1. (a) Leading-order diagram for hadronic production from the  $\psi$ . (b) Diagram leading to the production of direct photons at the  $\psi$ .

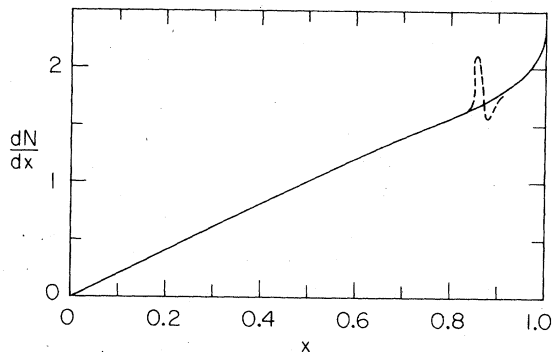


FIG. 2. Inclusive direct-photon momentum distribution, calculated to lowest order in QCD, as a function of  $x$ . Dashed curve shows the effect of resonance production in the final state.

the leading-order diagram. It is expected that the observed distribution will be softer than the leading-order prediction since radiative effects and the masses of the final-state hadrons have not been considered, but no calculation including these effects has been made. A similar calculation for the decay width of a heavy-quark-anti-quark bound state indicates that higher-order effects are of the same magnitude as lower-order terms,<sup>5</sup> thus making it difficult to provide accurate theoretical predictions.

## II. EXPERIMENTAL APPARATUS

The data were collected with the Mark II magnetic detector at the SLAC  $e^+e^-$  storage-ring facility SPEAR at energies near the peaks of the  $\psi(3095)$  and  $\psi'(3684)$  resonances. A brief description of the detector is presented here. Details can be found in Ref. 6.

A schematic of the Mark II magnetic detector is shown in Fig. 3. Charged tracks are reconstructed from hits in the 16 cylindrical drift-chamber<sup>7</sup> layers which provide solid angle coverage over 85% of  $4\pi$  sr. The azimuthal coordinates of charged tracks are measured to an rms accuracy of approximately  $220 \mu\text{m}$  at each layer. The polar coordinates are determined from the 10 stereo layers oriented at  $\pm 3^\circ$  to the beam axis. The charged-particle rms momentum resolution can be expressed as

$$\delta p/p = [(0.015)^2 + (0.005p)^2]^{1/2},$$

where  $p$  is the momentum in GeV/c.

The 48 time-of-flight (TOF) scintillation counters which surround the drift chamber provide timing information over 75% of  $4\pi$  sr. The rms time resolution is 0.30 ns for hadrons. The average flight path of 1.85 m provides a separation of pions from kaons up to momenta of 1.35

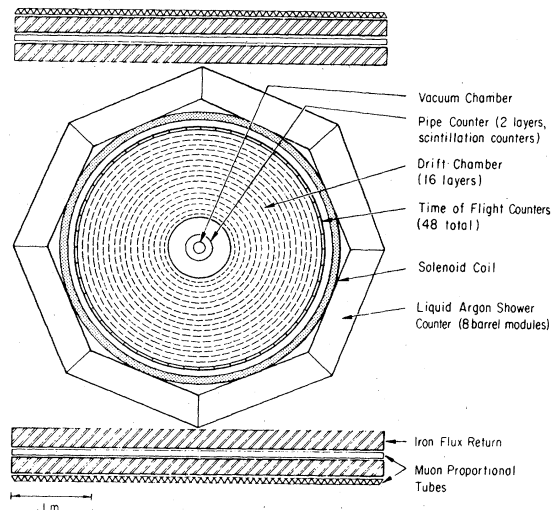


FIG. 3. Schematic of the Mark II magnetic detector looking along the beam direction. Not shown are additional muon proportional counters on both sides of the detector and the endcap shower counter modules.

GeV/c at the  $1\sigma$  level.

Photons are detected primarily in the eight lead-liquid-argon (LA) shower-counter modules<sup>8</sup> which surround the solenoid and cover approximately 64% of  $4\pi$  sr. (The LA also provides identification of high-energy electrons.) The shower-counter modules covering the endcap regions (not shown in Fig. 3) were not used in this analysis. The rms energy resolution for detected  $\gamma$ 's is given approximately by  $\delta E/E = 0.12E^{-1/2}$  ( $E$  in GeV). Photons which convert in the 0.06 radiation length of material preceding the drift-chamber layers (i.e., the vacuum pipe, the scintillation counters surrounding the vacuum pipe, and the lexan inner surface of the drift chamber) are reconstructed from measurement of the electron and positron tracks in the drift chamber. Although the detection efficiency is considerably less than for  $\gamma$ 's detected in the LA (due to the small conversion cross section), the energy resolution is much better.

The detector is triggered with a two-stage hardware trigger,<sup>9</sup> selecting (with efficiency greater than 99%) all interactions emitting at least two charged tracks, each with transverse momentum greater than 100 MeV/c, within the solid angle covered by the drift chamber. One of these tracks is required to be within the central region of the drift chamber which covers 67% of  $4\pi$  sr.

## III. DIRECT PHOTON PRODUCTION

We have measured the inclusive  $\gamma$  momentum distribution in the decay

$$\psi \rightarrow \gamma + X.$$

(1)

The analysis was based on a sample of 280 000 observed  $\geq 2$ -prong hadron events in  $e^+e^-$  annihilations near the peak of the  $\psi$  (3095). In order to eliminate QED interactions, events with only two oppositely charged prongs were required to be noncoplanar by at least  $20^\circ$ . The measured raw data has been corrected for  $\gamma$  detection efficiency and the average efficiency with which the detector should trigger on an event with a  $\gamma$  of given energy. We have restricted the analysis to  $\gamma$ 's detected in the LA shower counters.<sup>10</sup>

The  $\gamma$  detection efficiency (including geometric acceptance) was determined by Monte Carlo simulation of the electromagnetic shower development<sup>11</sup> in the LA shower-counter modules. This efficiency as a function of  $\gamma$  energy is shown in Fig. 4. In the Monte Carlo efficiency determination, the photon production angular distribution was assumed to be isotropic. Since the detector does not have uniform acceptance for all  $\theta$  (the polar angle of the  $\gamma$  with respect to the beam axis), a dependence of the production on  $\theta$  can result in a change in the detection efficiency from that shown in Fig. 4. The most general form for a single-particle angular distribution from the decay of a spin-1 object (e.g., the  $\psi$ ) created from the annihilation of an unpolarized  $e^+$  and  $e^-$  is

$$W(\theta, x) = 1 + \alpha_\gamma(x) \cos^2\theta, \quad (2)$$

where  $\alpha_\gamma(x) \leq 1$  for all values of  $x$ . In the most extreme case,  $\alpha_\gamma(x) = 1$  ( $-1$ ), a correction to the efficiency of  $-13\%$  ( $+25\%$ ) must be made to correct for the production angular distribution.

An estimate of the  $\gamma$  detection efficiency has also been obtained directly from the data. Two-constraint (2C) fits to two-prong and four-prong events at the  $\psi$  were made according to the hypotheses  $\psi \rightarrow \pi^+\pi^-\gamma(\gamma)$  and  $\psi \rightarrow \pi^+\pi^-\pi^+\pi^-\gamma(\gamma)$ , where a particle in parenthesis is meant to imply an unobserved particle. The  $\pi^0$  mass constraint was imposed on the  $\gamma(\gamma)$  system. The detection efficiency was calculated from the fraction of events in which the missing  $\gamma$  was observed and tracked in the LA. Corrections were made to correct for the geometrical bias imposed by the requirement that all charged particles be observed in the detector. These efficiencies, also shown in Fig. 4, agree well with the Monte Carlo efficiencies.

The trigger efficiency was measured from a sample of events taken near the peak of the  $\psi$ ' (3684). A sample of 92 000 events corresponding to the process

$$\psi' \rightarrow \psi \pi^+ \pi^- \quad (3)$$

was obtained by requiring that the missing mass from observed pairs of oppositely charged pions be consistent with the mass of the  $\psi(m_\psi)$ . The background from accidental combinations falling in the  $\psi$  mass region was estimated using events in bands on either side of the peak and subtracted. This sample of  $\psi$  events was identified purely from the  $\pi^+$  and  $\pi^-$  and has no trigger bias arising from the  $\psi$  decay. (The  $\pi^+\pi^-$  system was required to satisfy the trigger requirement.) As a function of observed  $\gamma$  momentum  $p$ , the trigger efficiency was calculated as the fraction of events which should satisfy the trigger requirement after elimination of the recoiling  $\pi^+$  and  $\pi^-$  from the event. (The fact that the  $\psi$  was not produced at rest in this sample of events has no significant effect on the efficiency.) The resulting trigger efficiency as a function of  $x = 2p/m_\psi$  is shown in Fig. 5. This sample of events also provides an estimate of the fraction of  $\psi$  decays which should result in at least two noncoplanar charged prongs within the solid angle of the detector. From this, we calculate the number of produced  $\psi$  events corresponding to the 280 000 observed hadron events to be 435 000.

Figure 6 (solid points) shows the inclusive  $\gamma$  momentum distribution,  $(1/N_{\text{tot}})dN/dx$ , as a function of  $x$ , where  $N_{\text{tot}}$  is the total number of pro-

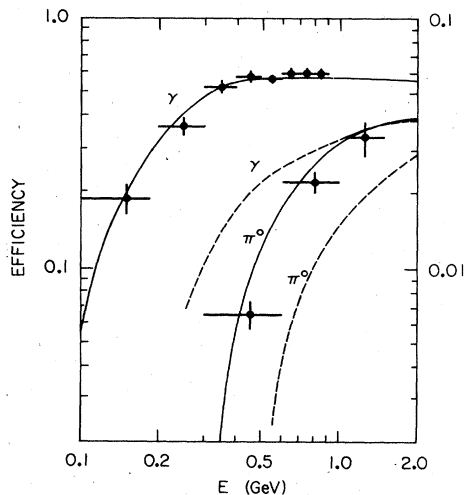


FIG. 4. Solid curves show the detection efficiency (including geometry) for  $\gamma$ 's and  $\pi^0$ 's detected in the LA as functions of energy (left ordinate). Dashed curves show the detection efficiency for  $\gamma$ 's which convert prior to entering the drift chamber and  $\pi^0$ 's reconstructed with one converted  $\gamma$  (right ordinate). Data points show efficiencies determined directly from the data.

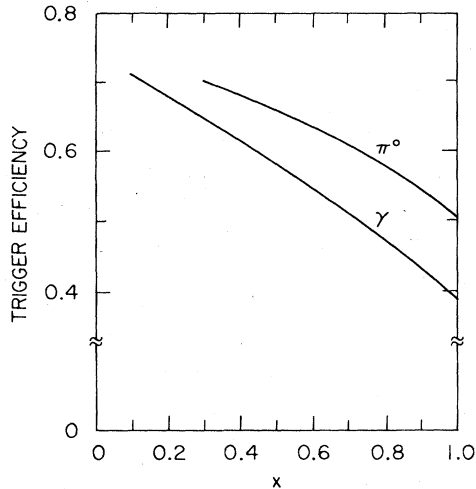


FIG. 5. Trigger efficiency as a function of  $x$  for events with observed  $\gamma$ 's or  $\pi^0$ 's detected in the LA.

duced  $\psi$  events for the data sample. The error bars represent the statistical errors only. Overall systematic errors are estimated to be less than  $\pm 20\%$  and may vary slowly with  $x$ . Corrections for trigger efficiency and  $\gamma$  detection efficiency have been made. As the cross section for hadron production is so much larger at the  $\psi$  than at center-of-mass energies, off-resonance, near the  $\psi$ , backgrounds from beam-gas interactions and radiative QED events are small. The major source of background is due to the  $e^+e^-$  final state in which one of the electrons radiates

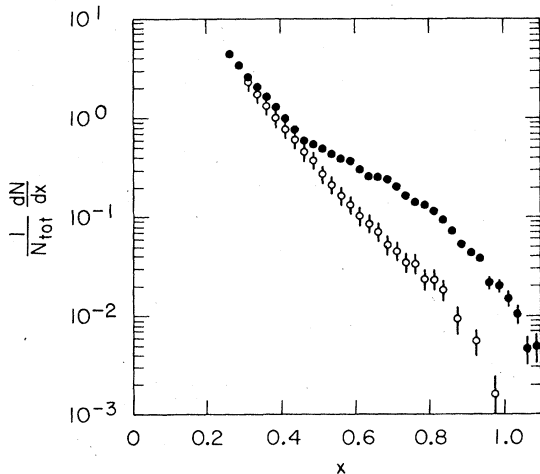


FIG. 6. Inclusive  $\gamma$  momentum distribution,  $(1/N_{\text{tot}})dN/dx$ , as a function of  $x$ . The solid data represent the measured  $\gamma$  spectrum for reaction (1) and the error bars are statistical only. The open points represent the  $\gamma$  spectrum predicted from measurement of the  $\pi^0$  and  $\eta$  distributions. The error bars on these points include both statistical and relative systematic errors as discussed in the text.

a photon (either internally or in passage through the detector). This background has been eliminated by removing events with a  $\gamma$  and two charged prongs, one of which is within a  $37^\circ$  cone opposite the  $\gamma$  and is identified as an electron with momentum greater than  $1.0 \text{ GeV}/c$ .

In order to extract the direct-photon signal from the total inclusive  $\gamma$  momentum distribution, we subtracted the contributions to this distribution from secondary-hadron decays. We estimated the  $\pi^0$  and  $\eta$  decay contributions from measurements of the inclusive  $\pi^0$  and  $\eta$  momentum distributions. Neutral pions and  $\eta$ 's were reconstructed by combining pairs of  $\gamma$ 's, each of which was required to have momentum greater than  $150 \text{ MeV}/c$ . This momentum cut eliminated most false photons found by the tracking program due to noise in the LA preamplifiers. Figure 7 shows the  $\gamma\gamma$  invariant-mass distribution for combinations with total momentum greater than  $1.2 \text{ GeV}/c$ . A clean  $\pi^0$  signal is observed over relatively little background. In addition, we observe a signal which is consistent in mass and width with expectations for an  $\eta$  signal. The momentum cut at  $1.2 \text{ GeV}/c$  greatly reduces the combinatorial background, but a  $\pi^0$  signal can be cleanly extracted from the background to below  $0.4 \text{ GeV}/c$  total momentum. However, we see no inclusive  $\eta$  signal for invariant-mass combinations with total momentum less than  $1.2 \text{ GeV}/c$ .

Pairs with invariant mass between  $0.075$  and  $0.200 \text{ GeV}$  were considered to be  $\pi^0$  candidates. The  $\pi^0$  signal was extracted after subtraction of the combinatorial background. As the background is momentum dependent (both in shape and normalization relative to the  $\pi^0$  signal), the data

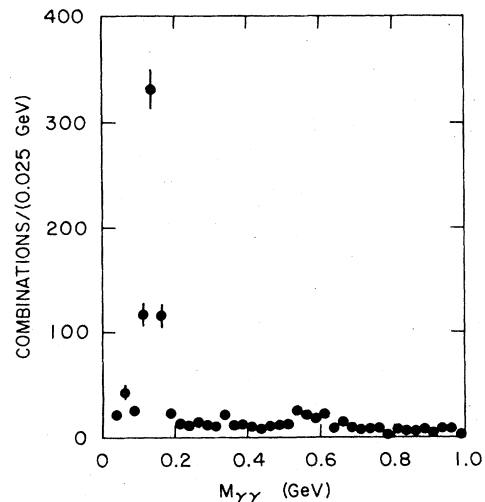


FIG. 7. Invariant-mass distribution for  $\gamma\gamma$  combinations with total momentum greater than  $1.2 \text{ GeV}/c$ .

were binned by momentum and the background subtraction was done independently for data in each momentum interval. The background shape was obtained by combining real photons and "pseudophotons" from the same event. Pseudophotons were created in the analysis program by pretending that charged particles were  $\pi^0$ 's and allowing them to decay into pairs of pseudophotons.<sup>12</sup> Resolution and efficiency effects were included in the generation of pseudophotons in order to simulate the effect of the detector on the produced- $\gamma$  momentum spectrum. Thus, the resulting pseudophoton momentum distribution corresponded well to the momentum distribution of observed photons from  $\pi^0$  decays. The background distribution was normalized to the data in the mass region between 0.3 and 1.0 GeV. The number of  $\pi^0$ 's was defined to be the difference between the number of measured  $\gamma\gamma$  combinations with mass between 0.075 and 0.200 GeV and the number of normalized background combinations in the same mass interval. It has been empirically determined that for this data, this technique of background generation provides a better representation of the background than the conventional technique of combining pairs of  $\gamma$ 's from different events.

The  $\pi^0$  detection efficiency, including a correction for the tails of the  $\pi^0$  which fall outside the specified mass cuts, was calculated by Monte Carlo techniques. The full electromagnetic-shower-development simulation was used in the Monte Carlo calculation to ensure that the effects of shower overlap were properly accounted for. In addition, all cuts used in the  $\pi^0$  reconstruction and data analysis were incorporated into the efficiency calculation. The  $\pi^0$  detection efficiency as a function of  $\pi^0$  energy is shown in Fig. 4. Also shown are measurements of the  $\pi^0$  efficiency as determined from 1C fits to the hypotheses  $\psi \rightarrow \pi^+\pi^-(\pi^0)$  and  $\psi \rightarrow \pi^+\pi^-\pi^+\pi^-(\pi^0)$ . The  $\pi^0$  detection efficiency was calculated from the fraction of events in which the missing  $\pi^0$  was observed, with corrections made for geometrical bias (similar to the corrections made in the measurement of the  $\gamma$  detection efficiency). However, these  $\pi^0$  efficiency measurements must be considered as lower limits since the decays  $\psi \rightarrow \pi^+\pi^-\gamma$  and  $\psi \rightarrow \pi^+\pi^-\pi^+\pi^-\gamma$  will successfully fit the corresponding hypothesis in which the  $\gamma$  is replaced by a  $\pi^0$ , but no  $\pi^0$  will be observed.

The trigger efficiency was determined for events with observed  $\pi^0$ 's in a manner similar to that used for determining the  $\gamma$  trigger efficiency. This trigger efficiency is shown in Fig. 5 as a function of  $x = 2p/m_\psi$ .

It should be emphasized that the extreme care

taken in the extraction of the  $\pi^0$  signal from the background is important only for small values of  $x$ . It is clear from the relatively small amount of background in Fig. 7 under the  $\pi^0$  peak that any method of background subtraction will give basically the same result. Thus, at large  $x$ , there is relatively little uncertainty associated with the  $\pi^0$  background subtraction.

Figure 8 shows the inclusive  $\pi^0$  momentum distribution  $(1/N_{\text{tot}})dN/dx$ . The error bars represent the statistical errors only. Overall systematic errors are estimated to be less than  $\pm 30\%$  and may vary slowly with  $x$ . Corrections for  $\pi^0$  detection efficiency and trigger efficiency have been made. A fit to the inclusive  $\pi^0$  momentum distribution between  $x=0.4$  and  $0.8$ , assuming a functional form proportional to  $e^{-bx}$ , gave a value for the slope of  $b=8.8 \pm 0.4$  (shown as the solid line in Fig. 8). The error includes estimated systematic uncertainties. This slope is consistent with the slope of the charged-pion spectrum at the  $\psi$ .<sup>13</sup>

The contribution to the  $\gamma$  momentum distribution from  $\pi^0$  decays was determined directly from the distribution in Fig. 8. In addition to the  $\pi^0$  decay contribution, there is an additional contribution to the inclusive  $\gamma$  momentum distribution from  $\eta$  decays.<sup>14</sup> To determine the  $\eta$  population, we have made least squares fits to the background-subtracted  $\gamma\gamma$  invariant-mass distributions in different momentum intervals. The functional form which was used in the fit consisted of a Gaussian, with mass fixed at the  $\eta$  mass and width as determined by Monte Carlo calculation of the mass resolution, over a linear background.

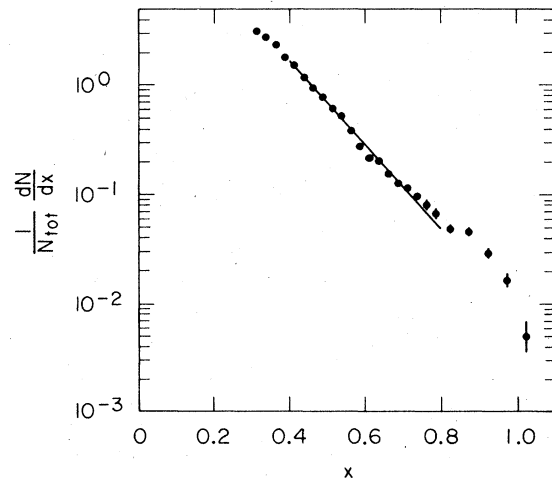


FIG. 8. Inclusive  $\pi^0$  momentum distribution,  $(1/N_{\text{tot}})dN/dx$ , as a function of  $x$ . The error bars represent the statistical errors only. Solid line represents fit described in text.

For momenta less than 1.2 GeV/c, only limits were set on inclusive  $\eta$  production (i.e., no significant signal was observed). We relate the inclusive  $\eta$  production to the inclusive  $\pi^0$  production as a function of momentum:

$$R_\eta(p) = B(\psi \rightarrow \eta + X)B(\eta \rightarrow \gamma\gamma)/B(\psi \rightarrow \pi^0 + X).$$

$R_\eta(p)$  is less than 0.10 for all momenta except for  $p > 1.2$  GeV/c, where  $R_\eta = 0.16 \pm 0.06$ . (This error is statistical only. Possible systematic effects due to errors in the assumptions made about the shape of the background are not included in this error.) From the measured value of  $R_\eta$  as a function of momentum, we estimated the  $\eta$  decay contribution to the  $\gamma$  momentum distribution.

A comparison between the measured  $\gamma$  momentum distribution and the  $\gamma$  momentum distribution predicted from the measured  $\pi^0$  and  $\eta$  distributions is shown in Fig. 6. It is seen that the predicted distribution is consistent with the measured distribution for  $x < 0.4$ , but at larger values of  $x$ , there is a clear excess of produced photons. The error bars on the predicted distribution include a systematic error of  $\pm 23\%$  representing possible systematic errors (see Table I) which are not common to both the measured and predicted  $\gamma$  momentum distributions. The major contributions to this error are the uncertainty in the  $\pi^0$  detection efficiency and the background subtraction. This error does not include correlated errors which affect the  $\gamma$  and  $\pi^0$  distributions similarly (e.g., overall normalization errors).

Figure 9 shows the direct-photon momentum distribution which was calculated by subtracting

the predicted distribution from  $\pi^0$  and  $\eta$  decays from the measured distribution. The data have been corrected for the deviation of the production angular distribution from isotropy. (This correction will be discussed shortly.) The error bars include both the statistical errors and the systematic errors in the difference between the measured and predicted distributions. The errors become small at large  $x$  because the  $\pi^0$  contribution is small and the error bars reflect only the statistical errors. Since the error bars at the lower values of  $x$  are dominated by the systematic errors, the extent of the error bars should be considered as defining an envelope within which the actual distribution lies. For  $x < 0.4$ , the errors become too large to provide meaningful information, and only for  $x > 0.5$  can a clear excess be demonstrated. It should be emphasized that because of the relatively small  $\gamma$  contribution from  $\pi^0$  and  $\eta$  decays at large  $x$ , rather large errors in our estimates of  $\pi^0$  and  $\eta$  production have a relatively small effect on the direct-photon rate. For instance, a factor-of-2 error in the amount of  $\eta$  production is well within the estimated systematic errors in the  $\pi^0$  momentum distribution.

In addition to the displayed error bars, there is a  $\pm 17\%$  systematic error on the distribution due to uncertainties in the  $\gamma$  detection efficiency, the number of produced  $\psi$  events, the trigger efficiency, and the production angular distribution of the direct photons. Table I explicitly lists these systematic errors.

The theoretical expectation for the direct-photon momentum distribution (convoluted with the energy resolution for  $\gamma$ 's detected in the LA) is also

TABLE I. Estimated systematic errors. Overall errors apply to both the  $\gamma$  and  $\pi^0$  distributions. Relative errors apply additionally to the  $\pi^0$  distribution.

Source	Error (%)	
	Overall	Relative
Number of produced events	$\pm 7$	
Trigger efficiency	$\pm 10$	$\pm 5$
$\gamma$ detection efficiency	$\pm 10$	
$\pi^0$ detection efficiency and background subtraction		$\pm 20$
Feed-down from lower $x$ due to resolution	$\pm 6$	
Shower-counter linearity <sup>a</sup>		$\pm 3$
Production angular distribution	$\pm 4$	
$\eta$ fraction <sup>b</sup>		$\pm 10$
Total <sup>c</sup>	$\pm 17$	$\pm 23$

<sup>a</sup> The overall error due to nonlinearity is absorbed into the  $\gamma$  detection efficiency uncertainty.

<sup>b</sup> This error only applied to the predicted  $\gamma$  distribution which includes both  $\pi^0$  and  $\eta$  contributions.

<sup>c</sup> The  $\pm 30\%$  systematic error on the  $\pi^0$  distribution comes from a combination of these two sets of errors.

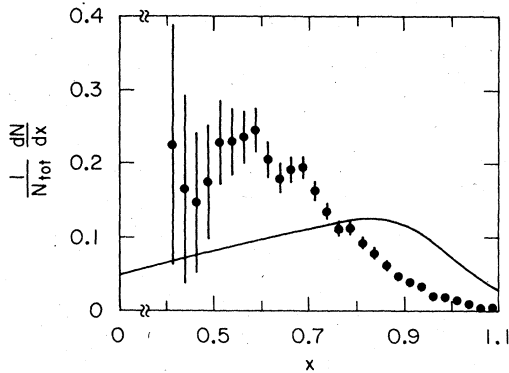


FIG. 9. Direct-photon momentum distribution. The solid curve is the leading-order QCD prediction convoluted with the LA photon energy resolution.

shown in Fig. 9. While the observed effect is seen to be of approximately the same magnitude as one might expect from theory, the observed distribution is softer. In particular, the data do not peak near  $x=1$ . This is not unexpected in light of the earlier discussion on second-order QCD corrections. Integrating the direct-photon momentum distribution from  $x=0.6$  to 1.0, we obtain an inclusive rate for direct-photon production of  $B(\psi \rightarrow \gamma + X) = (4.1 \pm 0.8)\%$ . This integrated cross section includes a  $-6\%$  correction (not included in the distribution shown in Fig. 9) for feed-down from lower  $x$  due to the energy resolution of the LA. The leading-order QCD calculation predicts an inclusive rate of 5% integrated over the same region in  $x$ .

It is assumed that the angular distribution of the direct photon signal is given by Eq. (2). The leading-order expression for  $\alpha_\gamma(x)$  is given by Koller and Walsh.<sup>3</sup> We do not have the statistics available to measure the angular distribution as a function of  $x$ , and can only measure an average value. Figure 10 shows the distribution of observed photons with  $x > 0.6$  as a function of  $|\cos\theta|$ . A least-squares fit to the data to Eq. (2) gives  $\alpha_\gamma = 0.14 \pm 0.12$ . (The curve in Fig. 10 shows the best fit to the data.) Approximately 25% of these photons are background from  $\pi^0$  or  $\eta$  decays. Analysis of the angular distribution of  $\gamma$ 's from observed  $\pi^0$  decays (in which both  $\gamma$ 's are observed) indicates that the distribution for  $\gamma$ 's from  $\pi^0$  background events is consistent with isotropy. Correcting for this background gives  $\alpha_\gamma = 0.18 \pm 0.18$  for the direct-photon events. An overall correction of 3% (assumed to be independent of  $x$ ) has been made to the data to account for the deviation of the observed angular distribution from isotropy (which was assumed in the original Monte Carlo efficiency calculation). The mean value of  $\alpha_\gamma(x)$ , convoluted with the mo-

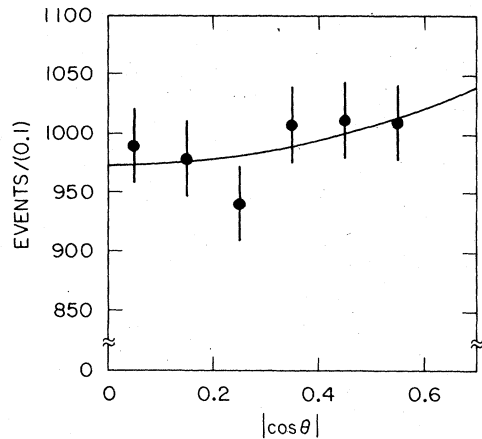


FIG. 10. Angular distribution of observed photons with  $x > 0.6$  as a function of  $|\cos\theta|$ . Curve is discussed in text.

mentum distribution from  $x=0.6$  to 1.0, is predicted to be approximately 0.3 from leading-order QCD calculations. Both this prediction and isotropy are in agreement with the data.

As a check on possible systematic errors and trigger bias problems, this analysis has been repeated with two different data samples which have inherently different systematic uncertainties. The first data sample consists only of events with photons which converted in the 0.06 radiation length of material preceding the drift chamber. No information from the LA system was used in the measurement of the inclusive  $\gamma$  momentum distribution from this sample of events. Neutral pions were reconstructed from combinations of a converted photon and a photon observed in the LA. The  $\gamma$  and  $\pi^0$  detection efficiencies (shown in Fig. 4 for comparison with the standard  $\gamma$  and  $\pi^0$  efficiencies) were calculated by the Monte Carlo method. As essentially all events with an observed converted photon should satisfy the trigger requirement (independently of whether the  $\gamma$  resulted from a  $\pi^0$  decay or not), there is no trigger bias in this data sample. In addition, this sample of events allows measurement of photon energies with very good resolution as the momentum resolution depends on the drift chamber resolution rather than the LA energy resolution. Empirically, we obtain an rms energy resolution of  $\delta E/E = 0.022E^{1/4}$  ( $E$  in GeV).

The second data sample consists of the statistically independent sample of  $\psi'$  (3684) cascade events [i.e., events produced in the process (3)]. Only photons observed in the LA were used in the analysis. Thus, the  $\gamma$  and  $\pi^0$  detection efficiencies are identical to the standard efficiencies. One minor problem results from the fact that the

$\psi(3095)$ 's were not produced at rest. Thus, after correction for detection efficiency, the  $\gamma$  and  $\pi^0$  momenta were Lorentz-transformed into the  $\psi$  center-of-mass frame. As described previously, this sample of events is also free of trigger bias.

Figure 11 shows the inclusive  $\gamma$  momentum distributions as determined by analysis of each of these two alternate data samples. The error bars represent the statistical errors only. Background from the  $e^+e^-$  final state in which one of the electrons radiates a photon has been removed as described above. This background is small for the sample of  $\psi'$  cascade events as the event selection eliminates QED interactions. In the sample of events with converted photons, there is also background from the reaction  $e^+e^-$

$\rightarrow \gamma\gamma$ . This background has been removed by elimination of events which have a high-energy  $\gamma$  detected in the LA opposite the converted  $\gamma$ , and no other charged tracks.

The inclusive  $\pi^0$  momentum distribution was determined independently for each of these two samples of events. As the statistics do not allow an independent estimate of  $\eta$  production from these data, the ratio of  $\eta$  to  $\pi^0$  production determined earlier was assumed in order to estimate the amount of  $\eta$  production. These distributions were used to estimate the contributions to the  $\gamma$  momentum distributions from  $\pi^0$  and  $\eta$  decays. The resulting predicted distributions are compared with the data in Fig. 11.

Figure 12 shows the direct-photon momentum distributions which were obtained by subtracting the predicted distributions from  $\pi^0$  and  $\eta$  decays from the measured distributions. The error bars include both the statistical and relative systematic

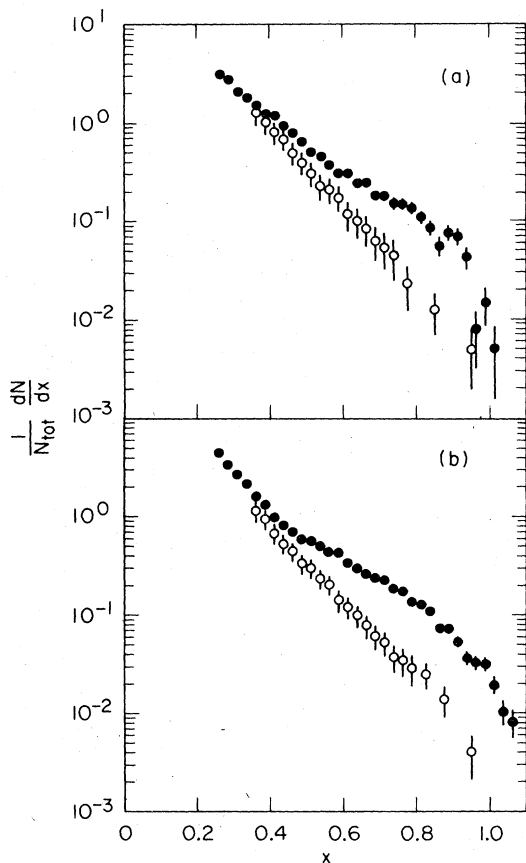


FIG. 11. Inclusive  $\gamma$  momentum distributions, as functions of  $x$ , from (a) events with converted photons and (b)  $\psi'$  cascade events. The solid data points represent the measured  $\gamma$  spectra and the error bars are statistical only. The open points represent the  $\gamma$  spectra predicted from measurement of the  $\pi^0$  and  $\eta$  distributions. The error bars on these points include both statistical and relative systematic errors.

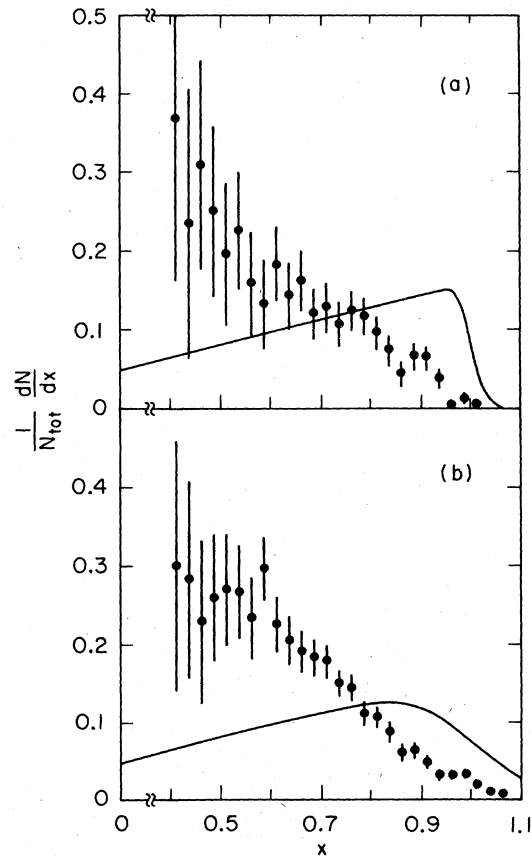


FIG. 12. Direct-photon momentum distributions from (a) events with converted photons and (b)  $\psi'$  cascade events. The solid curve is the leading-order QCD prediction convoluted with the energy resolution in each case.

errors. A comparison between the QCD prediction and the data is shown in each case. Integrating these distributions from  $x=0.6$  to 1.0, we obtain inclusive rates of  $B(\psi \rightarrow \gamma + X) = (3.9 \pm 1.2)\%$  from events with converted photons and  $B(\psi \rightarrow \gamma + X) = (4.4 \pm 1.0)\%$  from  $\psi'$  cascade events. The second number includes a correction ( $-6\%$ ) for feed-down due to the LA resolution, and both numbers have been corrected ( $+3\%$ ) for the effect of the assumed direct-photon angular distribution on the detection efficiency.

In summary, all three analyses give consistent results for both the momentum distribution and the integrated rate for direct-photon production. It should be emphasized that this consistency is not trivial. In particular, the analysis which incorporated converted photons, rather than photons observed in the LA, provides the best check that there are not subtle systematic problems which would simulate a direct-photon signal. First, use of the converted photon sample circumvents possible problems with reconstruction of photons in the shower counters or problems arising from linearity or resolution effects of the LA system. Second, the sample of converted photons ensures that the observed signal is due to photons and not due to contamination from neutrons or  $K_L$ 's. Finally, use of either of the two alternate data samples eliminates questions about the trigger efficiency.

Because the statistical accuracy of the first method of analysis is the best, we take that result as the best measurement from this experiment with  $B(\psi \rightarrow \gamma + X) = (4.1 \pm 0.8)\%$  for  $x > 0.6$ . This distribution (from Fig. 9) is shown in Fig. 13 compared to the results of Ronan *et al.*<sup>2</sup> Although the results of Ronan *et al.* are slightly lower than our results for  $x < 0.75$ , the two experiments are consistent within overall systematic

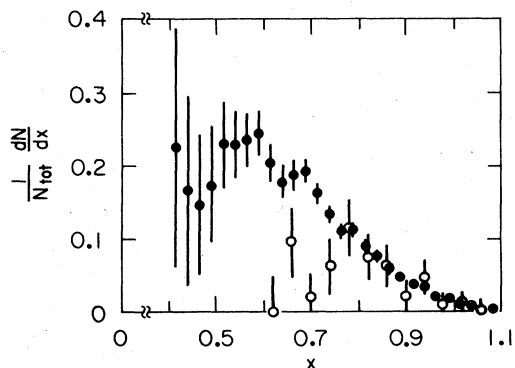


FIG. 13. Direct-photon momentum distribution from this experiment (solid points) and from Ref. 2 (open points).

errors. (Only statistical errors are shown in the figure.)

A final comparison can be made between the observed rate of inclusive  $\gamma$  production in this experiment and the previously measured rates for exclusive radiative transitions from the  $\psi$  to the  $\pi^0$ ,  $\eta$ ,  $\eta'$ ,  $f$ , and  $E(1420)$ .<sup>15</sup> These transitions account for a total of approximately 1% of all  $\psi$  decays. Thus, a large fraction of direct photon production at large  $x$  can be accounted for by known exclusive final states.

#### IV. CHARGED-PARTICLE MULTIPLICITY

We have measured the mean charged-particle multiplicity for the hadronic system  $X$  produced in reaction (1) as a function of the mass of the hadronic system ( $M_X$ ). The analysis was based on the sample of 280 000 observed  $\geq 2$ -prong hadron events described previously.

Events were grouped according to the observed photon energy:  $0.8 \leq E < 0.9$  GeV,  $0.9 \leq E < 1.0$  GeV,  $1.0 \leq E < 1.2$  GeV, and  $E \geq 1.2$  GeV. (Note that the mass of the recoil system is uniquely determined by the photon energy.) For each of the four sets of events, we determined the observed charged-particle multiplicity distribution for events which triggered the detector with two or more charged prongs. The produced charged-particle multiplicity distribution was obtained by an "unfold" procedure from the observed distribution.<sup>16</sup> This procedure basically consisted of solving the set of equations.

$$N_q = \sum_p \epsilon_{qp} \tilde{N}_p, \quad (4)$$

where  $N_q$  is an array giving the number of detected events of each prong multiplicity,  $\tilde{N}_p$  is an array giving the number of produced events of each prong multiplicity, and  $\epsilon_{qp}$  is a matrix giving the probabilities that an event with  $p$  produced charged prongs will be detected with  $q$  charged prongs. The solution for the array  $\tilde{N}_p$  was determined by maximum likelihood technique. (As the trigger requires two charged particles, we cannot determine  $\tilde{N}_0$ , the number of produced events with no charged particles.)

As a substantial fraction of the detected  $\gamma$ 's resulted from  $\pi^0$  decays, a three-step procedure was required to extract the produced charged-particle multiplicity distribution associated with the direct-photon events. The first step consisted of solving (unfolding) the system of Eqs. (4) for events with observed  $\pi^0$ 's. Events were grouped according to the observed  $\pi^0$  energy (rather than the observed  $\gamma$  energy), and for each energy, the observed multiplicity distribution was unfolded to give the produced multiplicity dis-

tribution. Only events with observed  $\pi^0$ 's (i.e., both  $\gamma$ 's observed) were used. The matrix  $\epsilon_{qp}$  (as determined by a Monte Carlo simulation to be described shortly) was calculated to give the probabilities that an event with a  $\pi^0$  of given energy and  $p$  produced charged prongs will be detected with  $q$  charged prongs. Hence, the  $\pi^0$  detection efficiency was included in these probabilities. (However, resolution effects, both for  $\pi^0$ 's and  $\gamma$ 's, were ignored.)

From this set of produced multiplicity distributions, a straight application of (4), with  $\epsilon_{qp}$  defined to give the probabilities that an event with a produced  $\pi^0$  will be detected with a  $\gamma$  of given energy (i.e., the  $\pi^0$  will not necessarily be detected), gave the background multiplicity distributions for nondirect photon events. As a  $\gamma$  of given energy can be produced in the decay of a  $\pi^0$  with any energy greater than the energy of the  $\gamma$ , the background multiplicity distributions were actually obtained by summing the distributions corresponding to  $\pi^0$ 's of all relevant energies, weighted by the appropriate  $\pi^0$  inclusive cross sections.

The final step consisted of subtracting the background multiplicity distribution obtained in the previous step (for each group of  $\gamma$  energies) from the observed multiplicity distribution. This distribution corresponds to the multiplicity distribution for direct-photon events only. This distribution was then unfolded, using still another  $\epsilon_{qp}$  which gave the corresponding direct-photon probabilities, to get the produced charged-particle multiplicity distribution.

The  $\epsilon_{qp}$  arrays used in the three steps were based on identical physics models for the hadronic system recoiling against the  $\pi^0$  or  $\gamma$ . The main differences in the probabilities arose because of the different efficiencies for detecting  $\gamma$ 's and  $\pi^0$ 's in the final state. The final-state hadrons from the decay of the recoiling system were generated according to a Lorentz-invariant phase-space model. Only systems containing charged and neutral pions were produced. The charged- and neutral-pion multiplicities were specified by separate Poisson distributions. Thus, two parameters served to totally specify the model, the mean total multiplicity and the ratio of the number of charged to neutral pions.<sup>17</sup> For a selected value of the mass of the hadronic system, the production model parameters (for both models) were determined from extrapolation of parameters obtained in fits to  $e^+e^-$  annihilation data at higher center-of-mass energies<sup>18</sup> down to energies corresponding to the invariant mass of the hadronic system. The parameters at these higher energies were determined by requiring

that the model yield the observed charged-particle mean momentum and mean multiplicity for detected events. Figure 14 shows the charged-track momentum distribution for a sample of events, each with an observed  $\gamma$  with energy between 0.9 and 1.0 GeV. The expected distribution based on a sample of Monte Carlo events, shown as the curve in the figure, agrees reasonably well with the measured distribution. Thus, we expect our calculated efficiencies to be reliable.

The resulting mean charged-particle multiplicity is shown in Fig. 15 as a function of  $M_X$ . (Produced states with no charged particles are not included in the average.) The error bars on the data reflect only the statistical errors and the errors resulting from the unfold procedure. Additional systematic errors due to the uncertainty in the background subtraction and the model used in the Monte Carlo event generation are not shown and are estimated to be less than  $\pm 15\%$ .

According to the theoretical ideas presented earlier, the system recoiling against the direct photon arises from a 2-gluon intermediate state. If one is to take these ideas literally, it is of interest to compare this system with the corresponding  $q\bar{q}$  system produced in  $e^+e^-$  annihilations at center-of-mass energies ( $E_{c.m.}$ ) comparable to the invariant mass of the two-gluon (i.e., hadronic) system. Naive expectations are that the multiplicities produced from the two-gluon system should be greater than the multiplicities produced from  $q\bar{q}$  systems.<sup>19</sup> We have investigated this possibility. Also shown in Fig. 15 are mean charged-particle multiplicities from

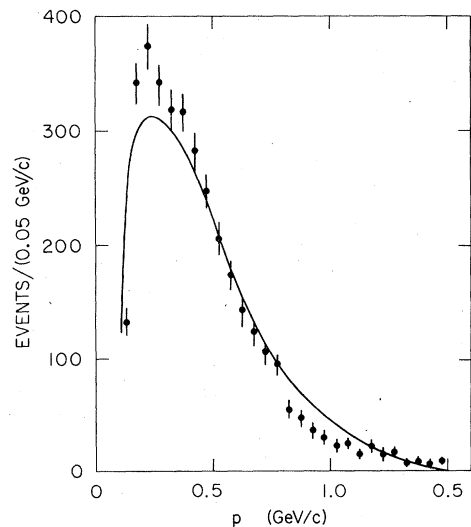


FIG. 14. Charged-track momentum distribution for events with  $\gamma$  energies between 0.9 and 1.0 GeV. Curve is distribution for Monte Carlo events.

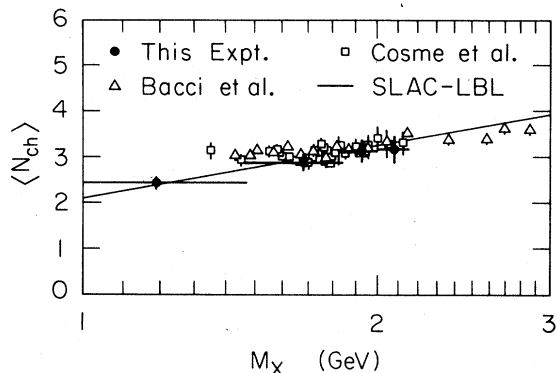


FIG. 15. Mean charged-particle multiplicity as a function of the invariant mass of the hadronic system. This data is compared with  $e^+e^-$  annihilation data of Cosme *et al.* (Ref. 20) and Bacci *et al.* (Ref. 21). The solid line is an extrapolation from higher-energy SPEAR data (Ref. 22).

low-energy  $e^+e^-$  annihilation data taken at the Orsay  $e^+e^-$  storage ring DCI<sup>20</sup> and the  $\gamma\gamma 2$  experiment<sup>21</sup> at ADONE compared to our direct-photon data. All error bars shown are statistical. At higher energy, similar measurements have been made with the SLAC-LBL magnetic detector<sup>22</sup> at SPEAR. The solid line in Fig. 15 is the extrapolated mean multiplicity distribution from the SLAC-LBL data. (The data are described well by the expression  $\langle N_{ch} \rangle = A + B \ln E_{c.m.}$  with  $A = 2.09$  and  $B = 1.67$ .) It is observed that the  $e^+e^-$  annihilation data and the direct-photon data yield consistent mean charged-particle multiplicities which fall on a universal curve of the form  $A + B \ln E_{c.m.}$ . The low-energy  $e^+e^-$  annihilation data show a slight excess in the region around 1.6 GeV, but analysis of the data shows that much of the cross section in this energy range is due to resonance production which has a large branching fraction into four charged pions.<sup>23</sup> This leads to a slight increase in the mean multiplicity.

Thus, we see no evidence from the charged-particle multiplicity data that the two-gluon system is different from the  $q\bar{q}$  system at these low energies. One possible explanation for this similarity is that the fragmentation of gluons into hadrons takes place by some mechanism similar to that shown in Fig. 16. Because of the small amount of phase space available to the gluons, they

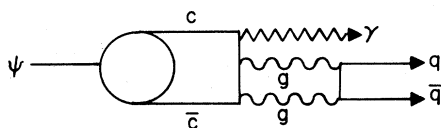


FIG. 16. Possible diagram for two-gluon annihilation in  $\psi$  decays.

annihilate immediately into a  $q\bar{q}$  pair which then fragments in a manner similar to  $s$ -channel  $q\bar{q}$  production in  $e^+e^-$  annihilation. One then expects to see no difference between the two-gluon and  $q\bar{q}$  multiplicities. (A similar annihilation of the three-gluon system from the direct hadronic decay of the  $\psi$  into a  $q\bar{q}$  pair would also explain the similarity of the inclusive properties of the hadronic final state on and off resonance at the  $\psi$ .)

## V. $K_S$ MULTIPLICITY

Because gluons couple to quarks independently of the quark flavor and photons couple with a strength proportional to the square of the quark charge, one expects production of leading  $d$  and  $s$  quarks to be suppressed relative to leading  $u$  quarks in  $e^+e^-$  annihilations, but not in final states resulting from the annihilation of two gluons. (We will ignore questions of phase-space suppression due to quark masses here.) Thus, one might expect the final states resulting from two-gluon annihilations to have larger kaon multiplicities, in particular  $K^0$  multiplicities, than the corresponding  $q\bar{q}$  states produced with the same invariant mass in  $e^+e^-$  annihilations.

We have measured the mean  $K_S$  multiplicity for the hadronic system produced in reaction (1) as a function of  $M_X$ .  $K_S$ 's were reconstructed from  $\pi^+\pi^-$  pairs observed in the detector. Figure 17 shows the  $\pi^+\pi^-$  invariant mass distribution for all events with photon energy greater than 0.8 GeV.  $K_S$  candidates are those pairs with invariant mass between 0.465 and 0.525 GeV. The background from accidental combinations falling in the  $K_S$  mass region was estimated using events on either side of the peak and subtracted.

As in the previous section, the data were grouped according to the observed photon energy. For each set of events, we determined the mean observed  $K_S$  multiplicity by dividing the number of observed  $K_S$ 's by the number of events. Due to the fact that essentially all events have either zero or one observed  $K_S$ , it was not necessary to use the complicated unfold procedure described above for obtaining the produced  $K_S$  multiplicity distribution. Rather, we used a Monte Carlo simulation to determine the efficiency for detection of a produced  $K_S$ . This allowed us to determine directly the mean produced  $K_S$  multiplicity from the mean observed  $K_S$  multiplicity. The Monte Carlo simulation was based on a simple model which assumed that the  $K_S$  momentum distribution follows the simple scaling law observed at higher energies.<sup>24</sup> This seems to be in basic agreement with the data, but the limited statistics do not allow a conclusive test. As es-

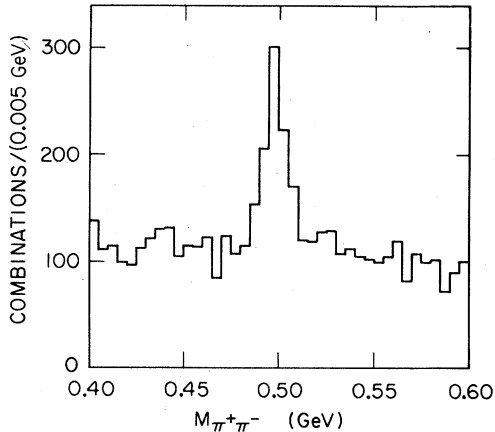


FIG. 17.  $\pi^+\pi^-$  invariant mass for events which contain a photon with energy greater than 0.8 GeV.

sentially all  $K_S$ 's observed in the detector satisfy the trigger requirement, the added complication of understanding the trigger efficiency was not required.

The resulting mean  $K^0$  multiplicity (assumed to be twice the  $K_S$  multiplicity) as a function of  $M_X$  is shown in Fig. 18. No background subtraction has been made for events with high-energy photons from  $\pi^0$  decays because of the limited statistics of the data with observed  $\pi^0$ 's. However, the correction is expected to be small, particularly for small values of  $M_X$ . The approximately  $\pm 20\%$  error bars reflect the statistical uncertainty in the number of  $K_S$ 's (approximately 100  $K_S$ 's per data point) and the systematic uncertainties associated with the  $K_S$  detection efficiency and background subtraction and the fact that no correction has been made for events in which the high-energy photon was produced from the decay of a  $\pi^0$  or  $\eta$ .

Also shown in Fig. 18 is the mean  $K^0$  multiplicity as a function of  $E_{c.m.}$  from  $e^+e^-$  annihilation data taken with the DM1 detector<sup>25</sup> at DCI. The published data is a measurement of  $R_{K^0} = 2\sigma_{K_S}/\sigma_{\mu\mu}$  (rather than a measurement of the  $K^0$  multiplicity), where  $\sigma_{K_S}$  is the measured  $K_S$  cross section and  $\sigma_{\mu\mu}$  is the theoretical  $\mu$ -pair production cross section. In order to determine the  $K^0$  multiplicity, the measured values of  $R_{K^0}$  were divided by  $R_{had} = \sigma_{had}/\sigma_{\mu\mu}$ , where  $\sigma_{had}$  is the measured hadronic cross section.  $R_{had}$  as a function of  $E_{c.m.}$  has been measured in a previous experiment at DCI.<sup>20</sup> In calculating the multiplicities shown in Fig. 18, we used values of  $R_{had}$  from this experiment, averaged over intervals of  $E_{c.m.}$ . The values used were  $R_{had} = 2.2$  for  $E_{c.m.} < 1.8$  GeV,  $R_{had} = 1.9$  for  $1.8 \leq E_{c.m.} < 2.0$  GeV, and  $R_{had} = 2.1$  for  $E_{c.m.} \geq 2.0$  GeV. The error bars on these

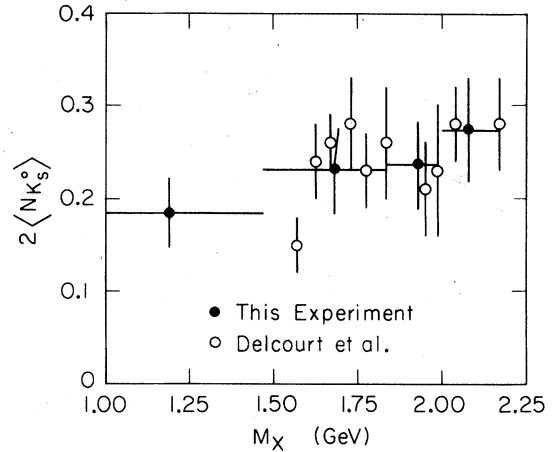


FIG. 18. Mean  $K^0$  multiplicity as a function of the invariant mass of the hadronic system. This data is compared with  $e^+e^-$  annihilation data of Delcourt *et al.* (Ref. 25).

data represent statistical errors only.

The two  $K^0$  multiplicity distributions agree well over the entire  $E_{c.m.}$  range. We see no evidence for a difference between the two-gluon and  $q\bar{q}$  final states. As mentioned previously, one might naively expect that the  $K^0$  multiplicity should be larger for two-gluon systems than for  $q\bar{q}$  systems. However, no account was taken of phase-space or propagator effects, and hence, these predictions should not be taken too seriously.

## VI. CONCLUSIONS

We have presented measurements of the inclusive  $\gamma$  and  $\pi^0$  momentum distributions at the  $\psi$ . We find a direct-photon component of the inclusive distribution for  $x > 0.5$  which cannot be explained by known decays of secondary hadrons. This direct photon production is consistent in magnitude with expectations from leading-order QCD predictions, but the momentum distribution is significantly different from the predicted distribution. However, second-order QCD corrections are known to be large, and are expected to soften the momentum distribution. This is in agreement with the trend observed in the data.

In an investigation of the differences between the assumed two-gluon system produced in this process and the  $q\bar{q}$  system produced off-resonance in  $e^+e^-$  annihilations, we measured the mean charged-particle and  $K_S$  multiplicities recoiling against the direct photons as functions of the invariant mass of the hadronic system. We found no difference between multiplicities observed in this data and data at the same invariant mass

( $E_{c.m.}$ ) in  $e^+e^-$  annihilations. Although the mean charged-particle multiplicity can be understood in terms of a model where the gluons annihilate immediately into a  $q\bar{q}$  pair, the consistency of the  $K_S$  multiplicities in the two final states is not as simple to understand. However, uncertainties due to phase-space and propagator effects, coupled with the large errors in the data, do not allow us to draw any firm conclusion.

## ACKNOWLEDGMENTS

We thank S. Brodsky and F. Gilman for helpful discussions. This work was supported primarily by the U. S. Department of Energy under Contracts Nos. DE-AC03-76SF00515 and W-7405-ENG-48. Support for individuals came from the listed institutions plus Deutsche Akademische Austauschdienst, Bonn and Ecole Polytechnique.

\*Present address: Vanderbilt University, Nashville, Tennessee 37235.

†Present address: CERN, Geneva, Switzerland.

‡Present address: California Institute of Technology, Pasadena, California 91125.

§Present address: Harvard University, Cambridge, Massachusetts 02138.

|| Present address: Universität Bonn, D-53 Bonn, Federal Republic of Germany.

¶Present address: Centre d'Etudes Nucléaires de Saclay, F-91190 Gif-sur-Yvette, France.

<sup>1</sup>G. S. Abrams *et al.*, Phys. Rev. Lett. **44**, 114 (1980).

<sup>2</sup>Another experiment [M. T. Ronan *et al.*, Phys. Rev. Lett. **44**, 367 (1980)] also sees evidence for production of direct photons at the  $\psi$ .

<sup>3</sup>T. Appelquist, A. De Rújula, H. D. Politzer, and S. L. Glashow, Phys. Rev. Lett. **34**, 365 (1975); M. S. Chanowitz, Phys. Rev. D **12**, 918 (1975); L. B. Okun and M. B. Voloshin, Institute of Theoretical and Experimental Physics, Moscow, Report No. ITEP-95-1976, 1976 (unpublished); S. J. Brodsky, T. A. DeGrand, R. R. Horgan, and D. G. Coyne, Phys. Lett. **73B**, 203 (1978); K. Koller and T. Walsh, Nucl. Phys. **B140**, 449 (1978).

<sup>4</sup>This calculation of  $\alpha_s$  is based on the ratio of the hadronic to the leptonic width of the  $\psi$  [see T. Appelquist and H. D. Politzer, Phys. Rev. Lett. **34**, 43 (1975)]. The predicted direct-photon contribution is included in the calculation as part of the total width of the  $\psi$ .

<sup>5</sup>R. Barbieri, E. d'Emilio, G. Curci, and E. Remiddi, Nucl. Phys. **B154**, 535 (1979).

<sup>6</sup>R. H. Schindler, Stanford Linear Accelerator Center Report No. SLAC-219, Ph.D. thesis, Stanford University, 1979 (unpublished).

<sup>7</sup>W. Davies-White *et al.*, Nucl. Instrum. & Methods **160**, 227 (1979).

<sup>8</sup>G. S. Abrams *et al.*, IEEE Trans. Nucl. Sci. **NS-25**, 309 (1978); G. S. Abrams *et al.*, IEEE Trans. Nucl. Sci. **NS-27**, 59 (1980).

<sup>9</sup>H. Brafman *et al.*, Stanford Linear Accelerator Center Report No. SLAC-PUB-2033, 1977 (unpublished).

<sup>10</sup>Details on the photon-track reconstruction and calibration can be found in C. A. Blocker, Lawrence Berkeley Laboratory Report No. LBL-10801, Ph.D. thesis, University of California, Berkeley, 1980 (unpublished).

<sup>11</sup>R. L. Ford and W. R. Nelson, Stanford Linear Accelerator Center Report No. SLAC-210, 1978 (unpublished).

<sup>12</sup>We have assumed that the charged particle and  $\pi^0$  momentum distributions from the  $\psi$  are similar. A pre-

liminary analysis shows no difference in the shapes of the two distributions over the range  $0.3 < x < 0.8$ . However, systematic uncertainties do not allow us to rule out a variation of 30% from the low end to the high end of the spectrum.

<sup>13</sup>W. Braunschweig *et al.*, Phys. Lett. **63B**, 115 (1976).

<sup>14</sup>The  $\gamma$  contribution from radiative decays of other secondary hadrons has been estimated to be small compared to the  $\eta$  contribution and negligible compared to the overall uncertainty in the  $\pi^0$  contribution.

<sup>15</sup>W. Bartel *et al.*, Phys. Lett. **64B**, 483 (1976); W. Bartel *et al.*, *ibid.* **66B**, 489 (1977); W. Braunschweig *et al.*, *ibid.* **67B**, 243 (1977); G. Alexander *et al.*, *ibid.* **72B**, 493 (1978); R. Brandelik *et al.*, *ibid.* **74B**, 292 (1978); D. L. Scharre, in *Current-Hadron Interactions*, edited by Trôn Thanh Vân (Editions Frontières, France, 1979), p. 219; R. Partridge *et al.*, Phys. Rev. Lett. **44**, 712 (1980); D. L. Scharre *et al.*, Phys. Lett. (to be published).

<sup>16</sup>A description of this procedure can be found in R. F. Schwitters, in *Proceedings of the 1975 International Symposium on Lepton and Photon Interactions at High Energies, Stanford, California*, edited by W. T. Kirk (SLAC, Stanford, 1976), p. 5.

<sup>17</sup>Note, however, that a given  $\epsilon_{cp}$  is a function of the momentum distribution of the produced charged tracks. Hence, to first order, it depends only on the total multiplicity used in the model.

<sup>18</sup>These parameters were obtained from the analysis described in G. Hanson *et al.*, Phys. Rev. Lett. **35**, 1609 (1975).

<sup>19</sup>S. J. Brodsky and J. F. Gunion, Phys. Rev. Lett. **37**, 402 (1976).

<sup>20</sup>G. Cosme *et al.*, Nucl. Phys. **B152**, 215 (1979).

<sup>21</sup>C. Bacci *et al.*, Phys. Lett. **86B**, 234 (1979).

<sup>22</sup>J. L. Siegrist, Stanford Linear Accelerator Center Report No. SLAC-225, Ph.D. thesis, Stanford University, 1979 (unpublished).

<sup>23</sup>This resonance data is reviewed in M. Spinetti, in *Current-Hadron Interactions*, edited by Trôn Thanh Vân (Editions Frontières, France, 1979), p. 263.

<sup>24</sup>V. Lüth *et al.*, Phys. Lett. **70B**, 120 (1977); R. Brandelik *et al.*, Nucl. Phys. **B148**, 189 (1979).

<sup>25</sup>B. Delcourt *et al.*, in *Proceedings of the 1979 International Symposium on Lepton and Photon Interactions at High Energies, Fermilab*, edited by T. B. W. Kirk and H. D. I. Abarbanel (Fermilab, Batavia, Illinois, 1980), p. 499.